1961

A numerical method of 1000-mb prognosis through prediction of thickness field

Chin, Ho-Chih; Kuan, Chuang-Tao; Pak, Ha Song

A NUMERICAL METHOD OF 1000-MB PROGNOSIS THROUGH PREDICTION OF THICKNESS FIELD

HO-CHIH CHIN
CHUANG-TAO KUAN
AND
HA SONG PAK

A NUMERICAL METHOD OF 1000-MB PROGNOSIS THROUGH PREDICTION OF THICKNESS FIELD

* * * * * * * * * * * * * * * * *

Ho-Chih Chin

Chuang-Tao Kuan

Ha Song Pak

A NUMERICAL METHOD OF 1000-MB PROGNOSIS THROUGH PREDICTION OF THICKNESS FIELD

by

Ho-Chih Chin //	Commander Republic of China Navy
Chuang-Tao Kuan	Lieutenant Commander Republic of China Navy
Ha Song Pak	Lieutenant (Junior Grade) Republic of Korea Navy

Submitted in partial fulfillment of
the requirements for the degree of

MASTER OF SCIENCE
IN
METEOROLOGY

United States Naval Postgraduate School
Monterey, California

1 9 6 1

A NUMERICAL METHOD OF 1000-MB PROGNOSIS THROUGH PREDICTION OF THICKNESS FIELD

by

Ho-Chih Chin

Chuang-Tao Kuan

Ha Song Pak

This work is accepted as fulfilling
the thesis requirements for the degree of
MASTER OF SCIENCE
IN
METEOROLOGY
from the
United States Naval Postgraduate School

ACKNOWLEDGEMENTS

The writers are indebted to Professor George J. Haltiner of the Department of Meteorology and Oceanography at United States Naval Postgraduate School for suggesting the topic, for outlining the way in which the study might be pursued, and for the assistance he rendered them.

They are also indebted to Lieutenant Commander Edward M. Carlstead of the Fleet Numerical Weather Facility, United States Navy, for the assistance he gave them during the course of investigation.

ABSTRACT

A two-level numerical prediction model incorporating terrain and non-adiabatic warming effects is tested. An attempt is made to determine the empirical coefficient(s) for each of three terms composing a prognostic equation designed to predict the 1000 to 500-mb thickness through the use of a digital computer.

The model is applied to three cases in April for a large part of the Northern Hemisphere. The predicted positions of most of the pressure systems were reasonably accurate; however the model tends to over-develop pressure centers. The effects of terrain and non-adiabatic warming were in accord with theoretical expectations; however, the excessive development dominated the numerical verification so that no significant improvement resulted from the inclusion of these refinements.

TABLE OF CONTENTS

LIST OF ILLUSTRATIONS

LIST OF ILLUSTRATIONS

TABLE OF SYMBOLS AND ABBREVIATIONS

α	Specific volume
C_d	Drag coefficient
C_p	Specific heat of dry air at constant pressure
C_v	Specific heat of dry air at constant volume
CDC	Control Data Corporation
∇	Two-dimensional del operator on a constant-pressure surface
d	Distance between adjacent grid points
f	Coriolis parameter
F	$F = \left[\frac{\partial}{\partial y}\left(C_d u \sqrt{u^2 + v^2} \right) - \frac{\partial}{\partial x}\left(C_d v \sqrt{u^2 + v^2} \right) \right]$
g	Acceleration of gravity
h	Thickness between 1000 mb and 500 mb
H_t	Terrain height
J	Jacobian
K_1	Coefficient of the advection term
K_2	Coefficient of the terrain term
K_3	Coefficient of the non-adiabatic term
K_4	Coefficient of the friction term
m	Map factor
mb	Millibar
θ	Potential temperature
p	Pressure
Q	Heat added per unit time per unit mass of air
R	Gas constant per gram of dry air
RMSE	Root-mean-square error
ρ	Density

t	Time
T	Temperature
T_s	Sea surface temperature
u	x-component of $\mathbf{V}_{g,o}$
v	y-component of $\mathbf{V}_{g,o}$
$\mathbf{V}$	Vector wind
$\mathbf{V}_g$	Geostrophic wind
$\mathbf{V}_t$	Vector wind at terrain height
$\mathbf{V}_T$	Thermal wind between p_o and p_5
ψ	Stream function
ω	dp/dt
w	Vertical velocity
ζ	Vertical component of relative vorticity
Z	Height of constant pressure surface

SUBSCRIPTS:

g	Geostrophic
1	Top of friction layer
s	Sea surface
t	Terrain
o	1000-mb
5	500-mb

1. INTRODUCTION

The availability of high-speed large-capacity electronic digital computers has long since made numerical weather prediction an operational reality. Notable success has been achieved at the 500-mb level. However, surface prognoses obtained by numerical integration techniques on the average have not equalled the accuracy obtained by subjective methods. Even with some relatively complex models, the degree of success has not corresponded to the degree of sophistication of the models. To improve the quality of surface prognosis, two alternatives seem to be feasible. One approach is to devise even more elaborate mathematical models in order to take into account as many pertinent weather parameters as possible. Perhaps new parameters which are not just a recombination of the familiar physical variables--pressure, temperature and humidity, will have to be introduced and measured to a high degree of accuracy on a synoptic time and space scale. Another alternative is to try quasi-empirical prediction models with a reasonable dynamical basis. In this paper a simple quasi-empirical 1000-mb prognostic model is derived and testing results are presented.

Since 500-mb prognoses from the barotropic model or its variations have been quite successful, a next logical step would be to devise a method to forecast the thickness field; and then through the predicted thickness arrive at the prognosis of some other level. In this experiment, a

technique for predicting the thickness field between 1000 mb and 500 mb is combined with results of the barotropic model currently in use by the Fleet Numerical Weather Facility. The predicted 500-mb stream field at every hour is applied in turn to generate a thickness between levels through a thickness-tendency equation. After sufficient iterations, a 24-hour 1000-mb prognostic contour map is obtained.

From the hydrostatic viewpoint, pressure is simply the weight of the air column above a particular level, and local changes in pressure may be thought of as the integrated density change in the air column. The density change can be described in terms of the temperature field which, in turn, can be expressed as a thickness change. The main feature of this model, the thickness-tendency equation, takes into account the temperature field, horizontal motions, and the vertical motions induced by terrain and surface stress.

Actually there is no inherent restriction on the choice of the 500-mb prediction equation. The thickness-tendency equation could be combined with any 500-mb model, though perhaps requiring some minor modifications in the programming. Obviously, if another 500-mb model is employed instead of the particular barotropic model used here, the results of testing may be quite different, and the empirical coefficients may not have the same values as obtained in this experiment.

2. Prognostic Model

The prognostic model is composed of two prediction equations. The first is the 500-mb stream-barotropic vorticity equation, the other is a thickness-tendency equation.

With the twisting term and vertical advection of vorticity omitted, the vorticity equation in (x,y,p,t) coordinates becomes

$$\frac{\partial \zeta}{\partial t} + \mathbf{V} \cdot \nabla (\zeta + f) = -(\zeta + f) \nabla \cdot \mathbf{V} \quad . \tag{1}$$

Due to the fact that at intermediate levels in the troposphere between 500 and 600 mb, the horizontal velocity divergence is normally relatively small and frequently may be neglected, the vorticity equation may be written in the form

$$\frac{\partial \zeta}{\partial t} + \mathbf{V} \cdot \nabla (\zeta + f) = 0 \quad . \tag{2}$$

Mere geostrophic approximation of (2) with

$$\mathbf{V}_g = -\frac{g}{f} \nabla z \times k \qquad \zeta_g = \frac{g}{f} \nabla^2 z$$

yields the barotropic quasi-geostrophic model

$$\nabla^2 \left(\frac{\partial z}{\partial t} \right) = -J \left(z, \frac{g}{f} \nabla^2 z + f \right) \tag{3}$$

where J is the Jacobian operator. Equation (3) has had considerable success in predicting the height field for 500 mb; but due to the velocity divergence inherent in the

geostrophic wind, an error commonly referred to as "spurious anticyclogenesis" is introduced. To remove this source of error, a non-divergent wind is used as follows:

$$\mathbb{V}_\psi = -\nabla\psi \times k \,, \qquad \mathcal{J} = \nabla^2\psi \,.$$

With these substitutions, equation (2) becomes:

$$\nabla^2\left(\frac{\partial\psi}{\partial t}\right) + J\left(\psi, \nabla^2\psi + f\right) = 0 \,. \tag{4}$$

A characteristic of the barotropic model as represented by (4) is that very long waves, say number 1, 2, and 3 with respect to a latitude circle, tend to retrogress at very high speeds, a phenomenon not observed in nature. To control this error, an additional term has been introduced. The result is the Helmholtz stream-barotropic equation

$$\nabla^2\frac{\partial\psi}{\partial t} - \mu\frac{\eta}{\bar{\varphi}}\frac{\partial\psi}{\partial t} = -\mathbb{V}_\psi\cdot\nabla\eta \tag{5}$$

where η is the absolute vorticity and μ is a constant.

The first law of thermodynamics and the Poisson's equation can be combined in the form

$$Q = c_p\frac{T}{\theta}\left(\frac{\partial\theta}{\partial t} + \mathbb{V}\cdot\nabla\theta + \omega\frac{\partial\theta}{\partial p}\right) \,. \tag{6}$$

Also from Poisson's equation and the equation of state, it follows that

$$\theta = aR^{-1}p^{c_v/c_p}1000^{R/c_p} \,, \tag{7}$$

which may be used in (6) to give

$$\frac{\partial \alpha}{\partial t} + \mathbf{V}\cdot\nabla\alpha + \frac{\alpha}{\theta}\frac{\partial\theta}{\partial p}\omega = \frac{Q\alpha}{c_p T} . \tag{8}$$

Finally replacing α in the first two terms on the left by means of the hydrostatic equation, and on the right through the equation of state yields

$$\frac{\partial}{\partial t}\left(\frac{\partial z}{\partial p}\right) = -\mathbf{V}\cdot\nabla\left(\frac{\partial z}{\partial p}\right) - \sigma\omega - \frac{QR}{c_p g p} . \tag{9}$$

Here $\sigma = \frac{1}{\theta}\frac{\partial\theta}{\partial p}\frac{\partial z}{\partial p}$ is the stability factor and is considered to be constant in space and time.

The "vertical velocity" may be considered to consist of three contributions, the large-scale vertical motion, the terrain-induced vertical motion and frictionally-induced vertical motion. Here these contributions will be represented by assuming ω to be of the form

$$\omega = \omega_5\left[1 - \left(\frac{p - p_5}{p_0 - p_5}\right)^2\right] - g\rho_0 k \frac{p}{p_0}\mathbf{V}_0\cdot\nabla H_t + \omega_l I \tag{10}$$

where

$$I = \begin{cases} \dfrac{p_0 - p}{p_3 - p_l} & \text{for} \quad p_l \leq p \leq p_0 \ ; \\ \\ 1 + \dfrac{p_l - p}{p_5 - p_l} & \text{for} \quad p_5 \leq p \leq p_l \ . \end{cases}$$

The first term on the right side of (10) is the parabolic distribution frequently assumed to be typical of large-scale pressure systems [1].

The second term of ω represents the terrain-induced vertical motion. Here the assumption is made that the surface vertical velocity w_0 is proportional to the horizontal wind and the gradient of terrain height at the surface; i.e., $w_0 = k\vec{V}_0 \cdot \nabla H_t$. Since $\omega_0 \doteq -g \rho_0 w_0$, it follows that $\omega_0 = -g \rho_0 k \vec{V}_0 \cdot \nabla H_t$. The terrain-generated vertical velocity is further assumed to decrease linearly with pressure; thus we arrive at the form in the second term.

The third term represents vertical motion induced by surface friction. Here ω_ℓ is the "vertical velocity" at top of the friction layer due to surface stress. It is assumed to have a simple distribution with respect to height which can be approximated linearly as shown in fig. 1.

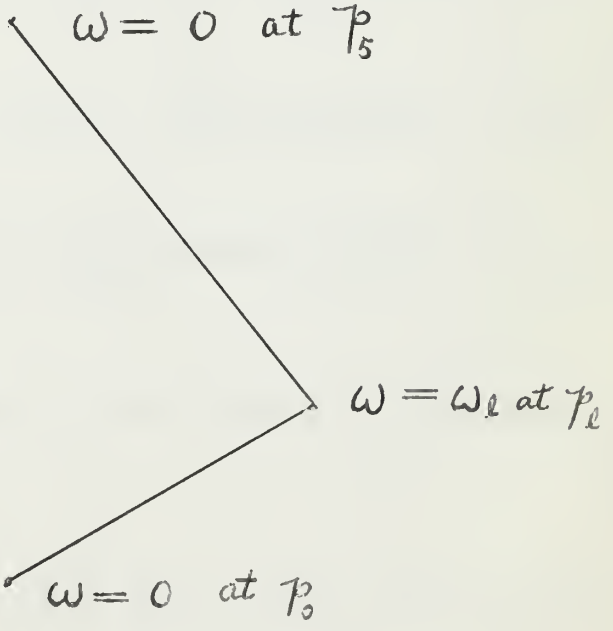

Figure 1. Profile of vertical velocity due to surface stress.

Cressman [2] deduced the following form for ω_l in terms of geostrophic surface wind and a drag coefficient:

$$\omega_l = \frac{\rho g}{f}\left[\frac{\partial}{\partial y}\left(C_d u\sqrt{u^2+v^2}\right) - \frac{\partial}{\partial x}\left(C_d v\sqrt{u^2+v^2}\right)\right] = \frac{\rho g}{f} F \quad (11)$$

where

$$F = \left[\frac{\partial}{\partial y}\left(C_d u\sqrt{u^2+v^2}\right) - \frac{\partial}{\partial x}\left(C_d v\sqrt{u^2+v^2}\right)\right] . \quad (12)$$

Here u and v are the x- and y-components of the geostrophic wind at 1000 mb, f is the coriolis parameter and C_d is the drag coefficient. The latter is mainly a function of the roughness of the underlying surface and stability in the micrometeorological layer, and has been determined for average conditions by Cressman for large-scale forecasting over the Northern Hemisphere.

Upon integration between P_0 and P_5 equation (9) becomes

$$\frac{\partial h}{\partial t} = -\bar{V}_5 \cdot \nabla h - \frac{2}{3}\sigma P_5 \omega_5 - \frac{3}{4} P_5 \sigma g \rho_0 k \bar{V}_0 \cdot \nabla H_t$$

$$- \frac{\sigma g F}{d \bar{f}}\left[\bar{\rho}_{0-1} + (P_5 - P_1)\bar{\rho}_{1-5}\right] + 0.691 \frac{R}{c_p g}\bar{Q} \quad (13)$$

where $\bar{Q}$ represents the amount of heat added to the layer per unit time.

If in equation (13) we

1. assume $\sigma P_5 \omega_5 = k \bar{V} \cdot \nabla h$ and combine it with the first term and affix a coefficient K_1;

2. combine coefficients in the second term and designate the combination as K_2;
3. assume $\overline{Q}$ is proportional to $\mathbf{V}_o \cdot \nabla T_s$, or $\overline{Q} = K_3 \mathbf{V}_o \cdot \nabla T_s$, where T_s is the sea-surface temperature; and
4. assume a reasonable pressure level as top of friction layer in the frictional term and designate the combined coefficient as K_4;

we arrive at:

$$\frac{\partial h}{\partial t} = -K_1 \mathbf{V}_5 \cdot \nabla h - K_2 \mathbf{V}_o \cdot \nabla H_t + K_3 \mathbf{V}_o \cdot \nabla T_s - K_4 F \quad (14)$$

This is the thickness-tendency equation, with the empirical coefficients to be determined through testing. The thickness equation together with the 500-mb stream-barotropic equation constitute the prognostic model.

The local rate of thickness change is thus seen to be due to the combined effect of thickness advection between layers, terrain effects, non-adiabatic heating and a frictional effect. Since cold advection is usually associated with adiabatic warming due to subsidence aloft and by heating from below in the surface layers, while warm advection is usually counteracted by cooling due to large-scale upward motion and in the surface layers by cooling from below, the coefficient K_1 might be expected

to have different values for cold and warm advection. This was borne out by the results of this numerical experiment.

The terrain term represents vertical motion induced by uneven terrain, and obviously it vanishes over oceans and level land.

The non-adiabatic term in the form $K_3 V_o \cdot \nabla T_s$ represents vertical diffusion of heat between air and surface water. For an air mass moving over warmer water, the surface temperature quickly adjusts to that of the surface water and rapid vertical diffusion of heat takes place. The rate of diffusion will normally increase with increasing horizontal wind which enhances the turbulence, and upward diffusion of heat will certainly continue as long as the water temperature increases downwind. For warm air moving over colder water the stability created by surface cooling in the lowest layer will tend to inhibit diffusive heat exchange. This suggests the empirical coefficient K_3 may also be assigned two values depending on the sign of $V_o \cdot \nabla T_s$.

The effects of surface stress about closed pressure systems may be summarized as follows:

Low: upward motion at top of friction layer, ω_ℓ negative; contribution to thickness tendency, negative.

High: downward motion at top of friction layer ω_ℓ positive; contribution to thickness tendency, positive.

Hesselberg and Friedmann found that the friction effect is at least two orders of magnitude smaller than some of the other terms in the vorticity equation. The assumption is made that it will also be quite small as compared to other terms in the thickness-tendency equation. Hence in the present experiment it was neglected. Thus equation (14) becomes

$$\frac{\partial h}{\partial t} = -K_1 \mathbf{V}_5 \cdot \nabla h - K_2 \mathbf{V}_t \cdot \nabla H_t + K_3 \mathbf{V}_0 \cdot \nabla T_5 \qquad (15)$$

where $\mathbf{V}_t$ represents the wind at the terrain height. Next the winds $\mathbf{V}_5$ and $\mathbf{V}_0$ in equation (15) are approximated by geostrophic values resulting in

$$\frac{\partial h}{\partial t} = -\frac{g}{f}\left[K_1 J(z_5, h) - K_3 J(z, T_5)\right] - K_2 \mathbf{V}_t \cdot \nabla H_t \qquad (16)$$

The wind at terrain height is computed by linear interpolation. On the assumption that wind hodograph is approximately a straight line between 1000 and 500 mb, $\mathbf{V}_t$ may be expressed in the form

$$\mathbf{V}_t = \mathbf{V}_5 - \left(\frac{z_5 - H_t}{h}\right)\mathbf{V}_T \qquad (17)$$

Thus the wind at terrain height is equal to the wind at 500-mb level minus some fraction of the thermal wind, and the fraction is the ratio of the surface/500-mb thickness to the 500/1000-mb thickness. With the geostrophic approximation for the wind and the letter A to designate $\left(\frac{Z_5 - H_t}{h}\right)$ it follows that

$$\mathbf{V}_t = \frac{g}{f}\left(-\frac{\partial Z_5}{\partial y}\mathbf{i} + \frac{\partial Z_5}{\partial x}\mathbf{j}\right) - A\frac{g}{f}\left(-\frac{\partial h}{\partial y}\mathbf{i} + \frac{\partial h}{\partial x}\mathbf{j}\right) \quad (18)$$

Hence the terrain term in equation (16) may be computed using two Jacobians. However, because of limited computer storage capacity, instead of the two Jacobian operations, the following transformation is made

$$\mathbf{V}_t \cdot \nabla H_t = \frac{g}{f}\left[\left(-\frac{\partial Z_5}{\partial y}\mathbf{i} + \frac{\partial Z_5}{\partial x}\mathbf{j}\right) - A\left(-\frac{\partial h}{\partial y}\mathbf{i} + \frac{\partial h}{\partial x}\mathbf{j}\right)\right] \cdot \nabla H_t \quad (19)$$

In finite differance form, the last expression becomes

$$\mathbf{V}_t \cdot \nabla H_t = \frac{m^2 g}{4fd^2}\left\{\left[-(Z_{5N} - Ah_N) + (Z_{5S} - Ah_S)\right](H_{tE} - H_{tN})\right.$$

$$\left. + \left[(Z_{5E} - Ah_E) - (Z_{5W} - Ah_W)\right](H_{tN} - H_{tS})\right\} \quad (20)$$

where the subscripts N, S, E and W are notations for the location of grid points. The quantity A has three variables, but may be simplified by taking standard atmospheric values for Z_5 and h without introducing too large an error. With the letters Z_{tN}, Z_{tS}, Z_{tE} and Z_{tW} to denote the quantities within the brackets in the final expression for $\mathbf{V}_t \cdot \nabla H_t$ above, equation (15) has the form

$$\frac{\partial h}{\partial t} = -\frac{h^2 g}{4 f d^2}\left\{K_1 J(Z_5, h) - K_3 J(Z_0, T_5)\right.$$

$$\left. + K_2\left[(Z_{tS} - Z_{tN})(H_{tE} - H_{tW}) + (Z_{tE} - Z_{tW})(H_{tN} - H_{tS})\right]\right\} \quad (21)$$

3. Procedure

Three days' data in April 1955 were tested. Prognoses were made for April 2nd, 3rd and 4th and were labeled as Cases 1, 2 and 3, respectively A CDC-1604 digital computer was employed for the computations over a 1977 point octagonal grid for the Northern Hemisphere poleward of 10N. At the end of each iteration, a predicted thickness is obtained at each grid point. This is subtracted from the prognostic 500-mb stream function to find the 1000-mb height. The final output is a predicted 1000-mb height field in a contour map form. The forward-difference method was used for calculation of $\frac{\partial h}{\partial t}$ for the first hour and a centered-difference method was used for succeeding hours. The forward and centered difference methods may be expressed respectively as

$$h_{t+\Delta t} = h_t + \left(\frac{\partial h}{\partial t}\right)_t \Delta t$$

and

$$h_{t+\Delta t} = h_{t-\Delta t} + \left(\frac{\partial h}{\partial t}\right)_t 2\Delta t .$$

A schematic block diagram of the thickness prediction program is given in fig. 2.

Using the computer, a "pillow" and a RMSE for each

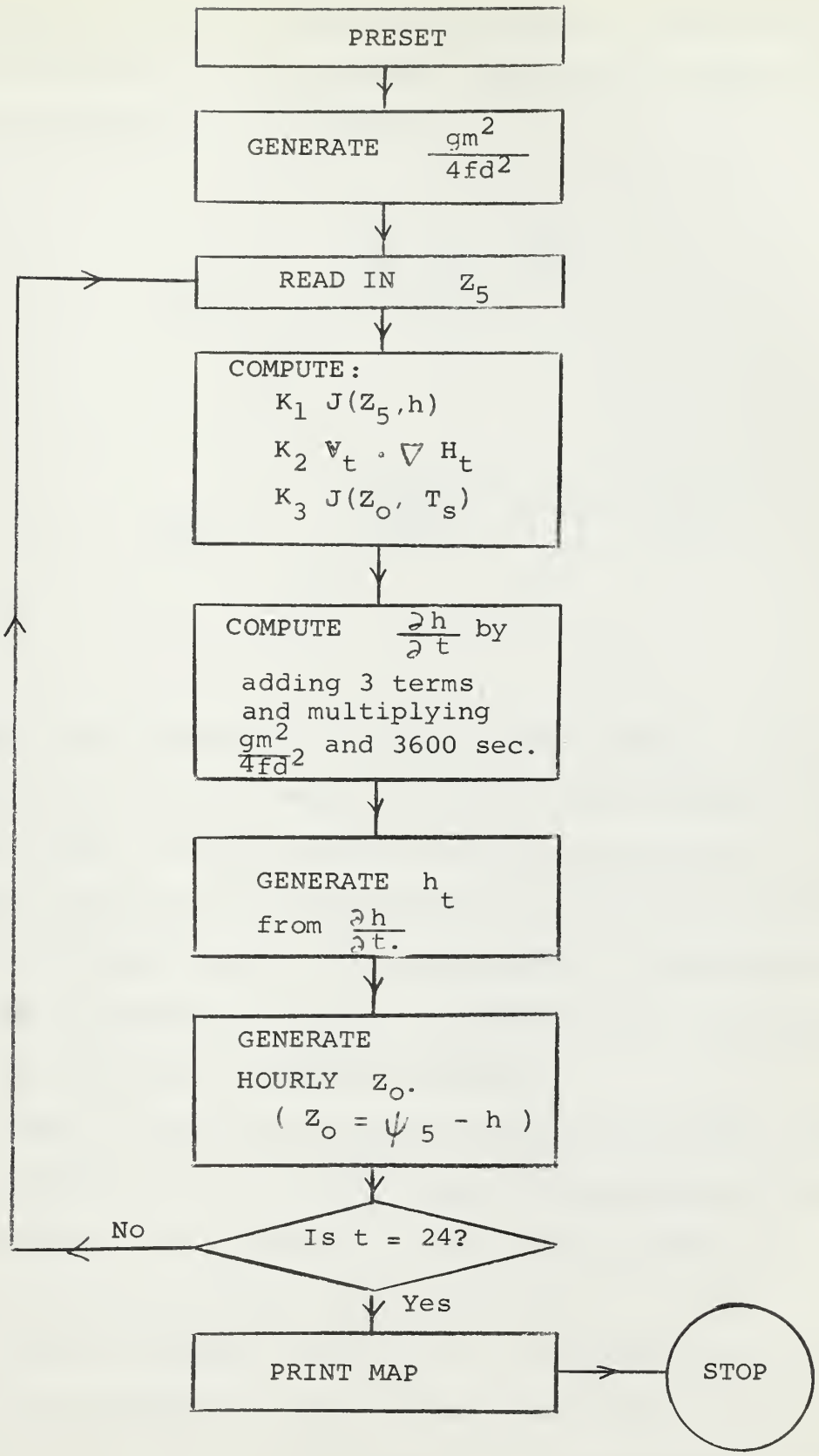

Figure 2. Schematic block diagram showing procedure.

prognostic map were computed by comparison with the actual map for verification purposes. The formulae used in computing the pillow and RMSE are

$$\text{pillow} = \frac{\sum_{n=1}^{\chi} (A-B)_n}{\chi}$$

$$\text{RMSE} = \sqrt{\frac{\sum_{n=1}^{\chi} [(A-B)-\text{pillow}]_n^2}{\chi}}$$

where A and B stand for predicted and verifying values, respectively, at the same grid point; and x stands for the total number of points differenced. Qualitatively, a pillow is the algebraic mean difference over the whole grid between the two fields A and B; while the RMSE is a numerical measure of the prognosis, and it reflects errors in position and in intensity of pressure systems.

Due to fictitious reflections on the boundary points and inaccuracies in the geostrophic approximation at low latitudes, it was decided to limit the verification to the areas north of the 20th latitude circle.

Since the major contribution to thickness change is due to the advection term, it was investigated first. Values of K_1 determined by previous investigators [3] were

used initially, then the value was varied to arrive at the best verification. Furthermore, since warm and cold advection did not necessarily give the same contribution to the predicted change in thickness, combinations of two different values were tried during the investigation of this term.

With the coefficients for the advection term tentatively determined, the investigation was carried on to find suitable coefficients for the terrain term. Only one coefficient of best fit was sought for the terrain term. During the investigation of this term, a smoothed terrain-height field is required in order to obtain the significant scale of vertical motion. Since the grid distance is about 380 km, any smaller-scale variation in the terrain field would not be included. For this reason, the smoothed terrain-height field data of J. Smagorinsky was used.

Finally, an investigation was conducted to find suitable coefficients for the non-adiabatic term. Two coefficients were sought for this term, one for heating and one for cooling. Values of K_3 determined by previous investigators [4] were also used initially in this case. The monthly-mean sea-temperature field of April was used during the investigation of the non-adiabatic term. This field was obtained by graphical addition of the monthly-mean air-temperature charts of April and the 3-month-mean air-sea temperature difference charts [5]. The resulting

temperature field is shown in fig. 10. The temperature field on the land area was included to facilitate the computations; however, these values did not enter into the final results.

4. Results and Discussion:

Figures 3 to 8 indicate the initial maps and the prognostic maps using different combinations of the terms forming the thickness-tendency equation. The isolines are drawn at intervals of 200 feet, and labeled in hundreds of feet. Case 3 has been chosen for illustration purposes because it gave the best results among the three cases tested, both in the prediction of the positions of the pressure centers and in numerical verifications.

By comparing figs. 4 and 5, it can be seen that the positions of the pressure systems are in close agreement with four exceptions, namely: the high over the east coast of Asia; the high off the west coast of the United States; the high over the Caspian Sea; and the high lying to the west of Gibraltar. Possible reasons for errors in their locations will be discussed at the end of this section. It was also of interest to notice that the positions of systems in the Atlantic Ocean were predicted more accurately than those in the Pacific Ocean.

Before discussing the coefficients found thus far in this investigation, it is necessary to mention two phenomena related to development. These phenomena are fictitious anticyclogenesis and cyclogenesis which predominated in all three cases tested. While no dynamical explanation could be determined from this investigation, it was apparent that the effect was due mainly to the advection term. Comparison of figs. 4 and 6 shows that most of the highs

were too high by an average amount of 200 feet, while most of the lows were too low by an average amount of 100 feet when the advection term was used alone to make the forecast. Since the major contribution to thickness change is due to the advection term, these phenomena invariably concealed the effects of a refinement like the non-adiabatic heat exchange in the numerical verification.

Aside from the effect of over-prediction by the advection term, it was found that the combination of coefficients 0.4 for warm advection and 0.5 for cold advection gave the best verification when this term is used alone to make the forecast. Other sets of coefficients, such as 0.8/0.9, 0.7/0.8, 0.5/0.5, 0.3/0.4, to mention only a few, gave larger RMSE values. Therefore, it was decided tentatively to use 0.4/0.5 as the coefficients of best fit for the advection term. The results of numerical verification for prognoses using the advection term only with coefficients of 0.4 for warm advection and 0.5 for cold advection are shown in Table 1.

Case Number	Pillow (ft)	RMSE (ft)
1 (0000Z April 2, 1955)	0	+189
2 (0000Z April 3, 1955)	+14	+171
3 (0000Z April 4, 1955)	+7	+168

Table 1. Results of numerical verification for prognoses using the thickness advection term only with coefficients of 0.4 for warm advection and 0.5 for cold advection.

For the investigation of the terrain term, verification by pillow and RMSE in Table 2 showed no improvement in RMSE when the terrain term was included in this model. In this connection, it should be noted that the empirically-determined best-fit coefficient of the terrain term is 0.01, while the maximum terrain-height gradient is about 12 times larger than the thickness gradient. Hence the terrain term contribution can be at most about 25% of the advection term. Also, less than half of the total area covered by the grid point is affected by the terrain term, while the pillow and RMSE were computed over the entire grid. Therefore, the actual contribution of the terrain term should be larger than that shown by RMSE.

In order to investigate the effects of the terrain-induced vertical motion in more detail, a differential analysis was made and presented in fig. 9. Here the difference between the forecast with thickness advection only (fig. 6) and that with both the terrain term and thickness advection (fig. 7) was computed. The isolines are drawn at intervals of 50 feet, and the figures labeled in tens of feet. Of the 20 closed isolines observed in fig. 9, 14 indicate a decreased error; 5 of them an increased error; and one, neutral. Thus, there are some areas where the terrain term does not give any improvement and, in fact, made the results worse. For example, over Greenland, the forecast made with the thickness advection alone over-intensifies the low, and with the inclusion of the terrain

Case Number	Pillow (ft)	RMSE (ft)
1 (0000Z April 2, 1955)	- 15	+ 191
2 (0000Z April 3, 1955)	+ 1	+ 172
3 (0000Z April 4, 1955)	- 7	+ 168

Table 2. Results of numerical verification for prognoses using advection and terrain terms with coefficients of 0.4 for warm advection, 0.5 for cold advection and 0.01 for the terrain term.

term, further deepening is observed on the leeward side of the mountain, giving an even poorer result.

Fourteen closed isolines of the 20 on the differential analysis showed a better forecast, with a two- to eight-mb improvement in the surface pressure field, when the terrain-induced vertical motion over land areas was included. These results indicate some justification for the inclusion of the terrain term in the model.

Since the terrain-induced vertical motion is a function of the wind component parallel to the terrain-height gradient as well as the terrain-height gradient itself, large values of terrain contribution may be expected in areas where above-mentioned values are large. In this respect, the test data available for this investigation were not favorable for a good evaluation of the terrain term. The synoptic maps show that the areas where the terrain gradient is large are mainly associated with small wind components parallel to the terrain-height gradient.

With only three days' data tested, no final conclusion can be reached regarding the terrain-induced vertical motion in this model at this time. Effects of the terrain-induced vertical motion were produced in areas where they were expected from dynamic considerations; however, the values are too small in general. This seems to suggest

that further experiments may indicate a larger coefficient for the terrain term with perhaps some other additive empirical factors.

The results of numerical verification for prognoses using advection and non-adiabatic terms are shown in Table 3. The eight blanks in Table 3 arose in cases where the forecast map was very much distorted, in contrast to the regular appearance of the remaining forecast maps. This erratic behavior was apparently connected with a malfunction of the magnetic tape units.

The coefficients of best fit for the non-adiabatic term, as shown in Table 4, were 10 for heating and 6 for cooling. They were chosen only because they provided the smallest pillow. The RMSE obtained by using this set of coefficients was $\pm$168 feet for case 3, which equaled exactly that obtained by using advection term alone for prognosis. As a matter of fact, Table 3 shows that the RMSE values increased when the coefficients were increased algebraically. Since it was mentioned earlier that the RMSE is a numerical measure of the accuracy of the forecast, it appears that the addition of the non-adiabatic term at best made no improvement in the forecast. Two arguments need to be made clear at this point. Firstly, fictitious anticyclogenesis and cyclogenesis by the advection term alone already have over-intensified most of the highs and the lows. Since the effect of the non-adiabatic term on the average is one order of magnitude less than that of

Coeff. heating/cooling	Case 1 (0000Z Apr 2, '55) Pillow (ft)	Case 1 RMSE (ft)	Case 2 (0000Z Apr 3, '55) Pillow (ft)	Case 2 RMSE (ft)	Case 3 (0000Z Apr 4, '55) Pillow (ft)	Case 3 RMSE (ft)
5/5	-15	+ 192	+ 1	+ 175	- 4	+ 167
5/10	- 6	+ 200	+ 9	+ 178	+ 3	+ 170
5/15	- 4	+ 205	+ 17	+ 182	+ 12	+ 178
5/20	+ 9	+ 209	+ 24	+ 188	+ 20	+ 187
10/5	- 4	+ 199	- 4	+ 177	-11	+ 168
10/6	- 2	+ 200	- 3	+ 177	- 1	+ 168
10/10	- 6	+ 215	+ 10	+ 183	+ 4	+ 177
10/15	———	———	+ 10	+ 184	+ 5	+ 178
10/20	0	+ 219	+ 18	+ 189	+ 13	+ 187
15/5	———	———	-11	+ 182	-18	+ 171
15/10	-23	+ 218	- 3	+ 184	- 9	+ 175
15/15	-13	+ 232	+ 4	+ 188	0	+ 182
15/20	- 8	+ 242	+ 11	+ 193	+ 7	+ 192
20/5	-43	+ 227	-18	+ 190	———	———
20/10	-32	+ 235	-10	+ 191	-15	+ 181
20/15	-22	+ 248	- 2	+ 196	- 7	+ 190
20/20	———	———	+ 5	+ 200	+ 1	+ 202
25/5	-42	+ 230	-20	+ 191	-24	+ 179
25/10	-33	+ 238	-10	+ 193	-16	+ 182
25/15	-23	+ 250	- 3	+ 197	- 8	+ 192
25/20	-13	+ 270	+ 4	+ 201	0	+ 204

(Continued on following page)

(Continued from previous page)

Coeff. heating/cooling	Case 1 (0000Z Apr 2,'55) Pillow (ft)	RMSE (ft)	Case 2 (0000Z Apr 3,'55) Pillow (ft)	RMSE (ft)	Case 3 (0000Z Apr 4,'55) Pillow (ft)	RMSE (ft)
30/5	———	———	-40	+ 218	-43	+ 200
30/10	———	———	-24	+ 219	-30	+ 204
30/15	———	———	-16	+ 221	-20	+ 218
30/20	———	———	- 8	+ 228	-12	+ 226

Table 3. Results of numerical verification for prognoses using advection and non-adiabatic terms with coefficients of 0.4 for warm advection and 0.5 for cold advection. The coefficients used for the non-adiabatic term are shown in the table.

Case Number	Coefficients used		Pillow (ft)	RMSE (ft)
1 (0000Z April 2, 1955)	K_1 (Warm advection)	0.4	- 22	+ 199
	K_1 (Cold advection)	0.5		
	K_2	0.01		
	K_3 (Heating)	10		
	K_3 (Cooling)	6		
2 (0000Z April 3, 1955)	K_1 (Warm advection)	0.4	- 10	+ 178
	K_1 (Cold advection)	0.5		
	K_2	0.01		
	K_3 (Heating)	10		
	K_3 (Cooling)	6		
3 (0000Z April 4, 1955)	K_1 (Warm advection)	0.4	- 9	+ 168
	K_1 (Cold advection)	0.5		
	K_2	0.01		
	K_3 (Heating)	10		
	K_3 (Cooling)	6		

Table 4. Results of numerical verification for prognoses using all three terms of the thickness-tendency equation, with coefficients as shown in the table.

the advection term, the advantage of including the non-adiabatic term would hardly appear. Secondly, for the non-adiabatic heat exchange, the zones of thermal concentration, where transformation of polar-continental air to polar-maritime air takes place, are really of primary concern. During the month of April, these zones of thermal concentration were found along the northeast coasts of Asia and North America. For the three cases investigated, cyclonic activity prevailed in these areas. With the 1000-mb lows already over-intensified by the advection term and with the flow oriented such that heating took place in these areas, the lows were intensified further. For example, the low off the east coast of Japan in case 3, where the lowest observed height was + 30 feet, the prognosis with the advection term alone gave a lowest height of - 170 feet while the non-adiabatic term decreased the lowest value further to - 250 feet. Thus, in spite of the fact that the behavior was in accord with theoretical expectations, the RMSE did not improve when the non-adiabatic term was included in this case.

In order to investigate the effect of the non-adiabatic term further, a differential analysis was made by subtracting a prognostic map with both advection and non-adiabatic terms included (fig. 8) from the one with only the advection term. This isolated the effect of the non-adiabatic term (fig. 6) and it was found that by using a coefficient of 10 for heating, the largest 24-hr

contributions by this term in areas of thermal concentration were -282 feet off the east coast of Nova Scotia, at 41N, 55W; and -230 feet off the west coast of Japan, at 40N, 134W.

Two possible sources of error warrant discussion. In the first place, the 1000-mb map was a relatively flat map, with the range of thickness values and 500-mb height much greater than the range of the 1000-mb height. Therefore, errors in the 500-mb height, when transmitted downward through the thickness, can cause serious deviations at the lower surface. Furthermore, it was obvious that one could not expect the locations of the pressure systems on the lower surface to be better than what the 500-mb prognosis can provide for this model. Secondly, the fact that the positions of the pressure systems were all better in the Atlantic Ocean than those in the Pacific Ocean, true in all three cases, was most probably due to the fact that weather reports in the Atlantic Ocean were more numerous and accurate than those in the Pacific Ocean. In other words, the initial data from which the prognosis was started could have been in error to a certain degree in the Pacific Ocean.

5. Conclusions:

Starting with a dynamical basis and utilizing the rapid computing capabilities of the CDC-1604 computer, empirical coefficients were found for each of the three terms of the prognostic equation designed to predict the 1000/500-mb thickness. By subtracting the predicted thickness from the 500-mb 24-hr prognosticated stream function, a 24-hr prognosis of the 1000-mb map was obtained. The fact that this model did provide a map with most of the pressure systems appearing at the right places is encouraging. Due to the relatively small sample tested, the empirical coefficients found thus far were not necessarily the best ones; but they will nevertheless provide a starting point for further investigations of a similar nature.

Improvements of the model might include the incorporation of certain empirical rules in order to remedy the phenomena of over-predicting cyclogensis and anticyclogenesis and the use of the weekly-mean sea-temperature field instead of the monthly mean. Furthermore, any improvement in the prediction of the 500-mb maps will give increased accuracy at 1000 mb. In conclusion, it is the opinion of the present investigators that this model can provide a first approximation in the preparation of the surface prognostic map.

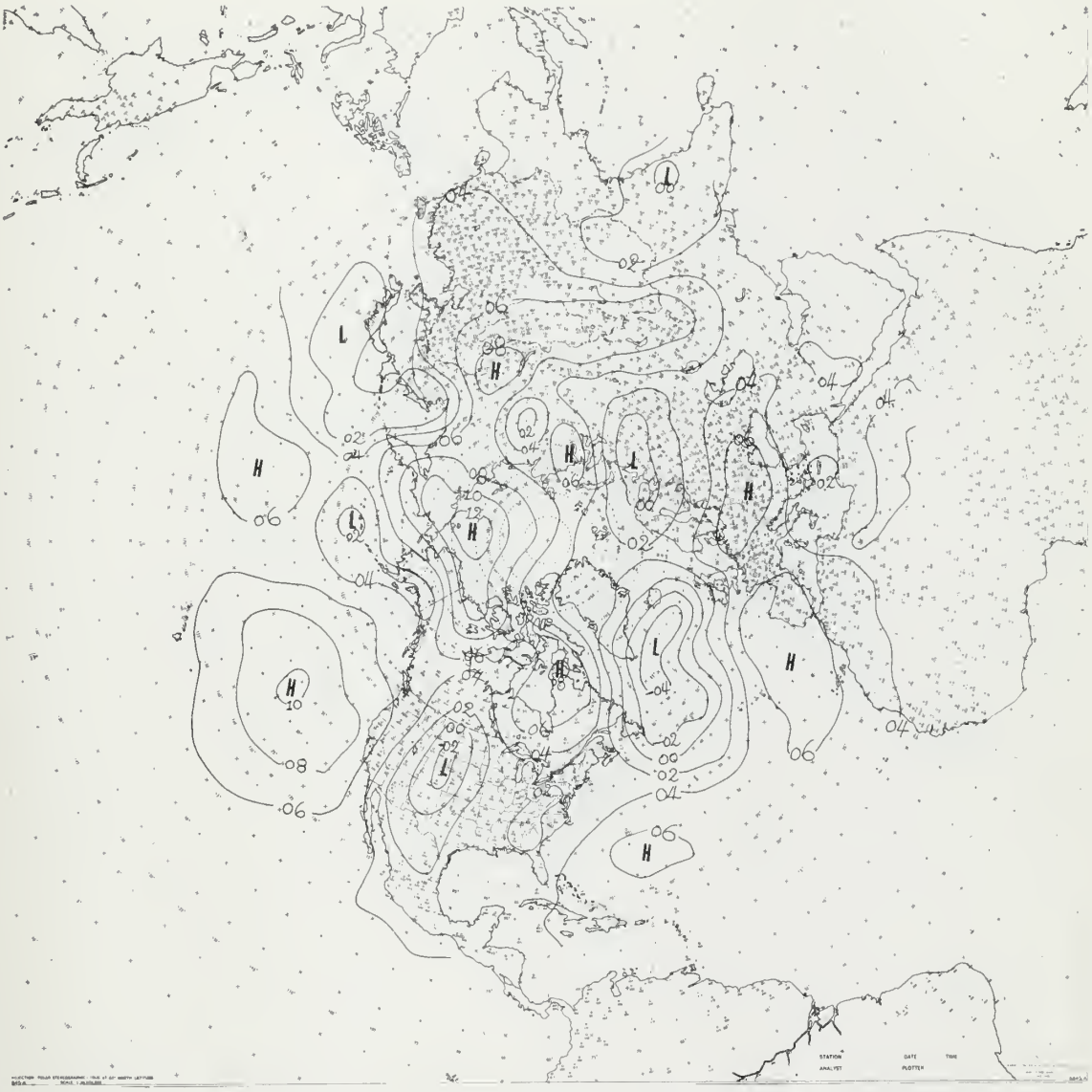

Figure 3. The 1000-mb map for 0000Z April 3, 1955.

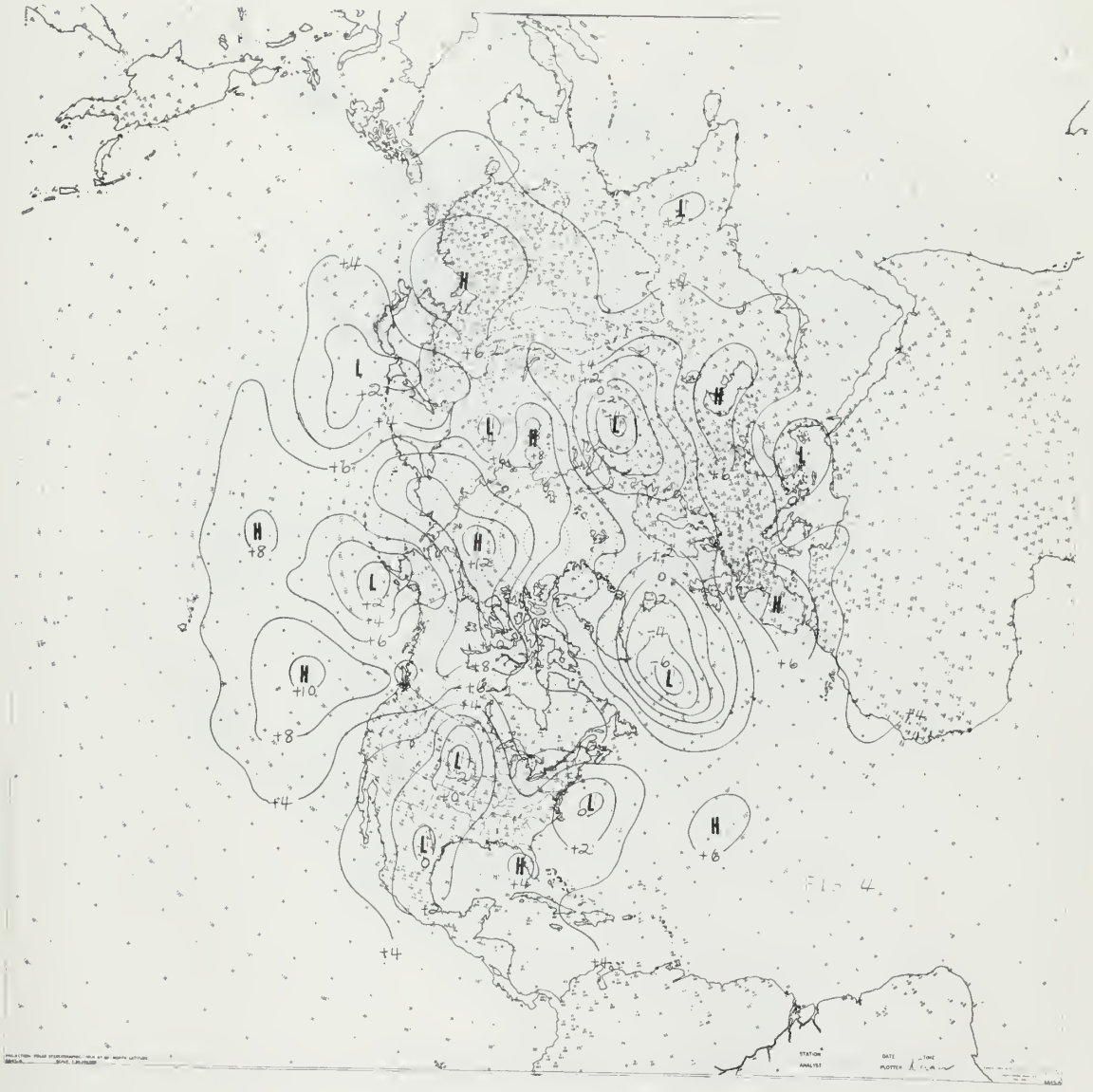

Figure 4. The observed map for 0000Z April 4, 1955.

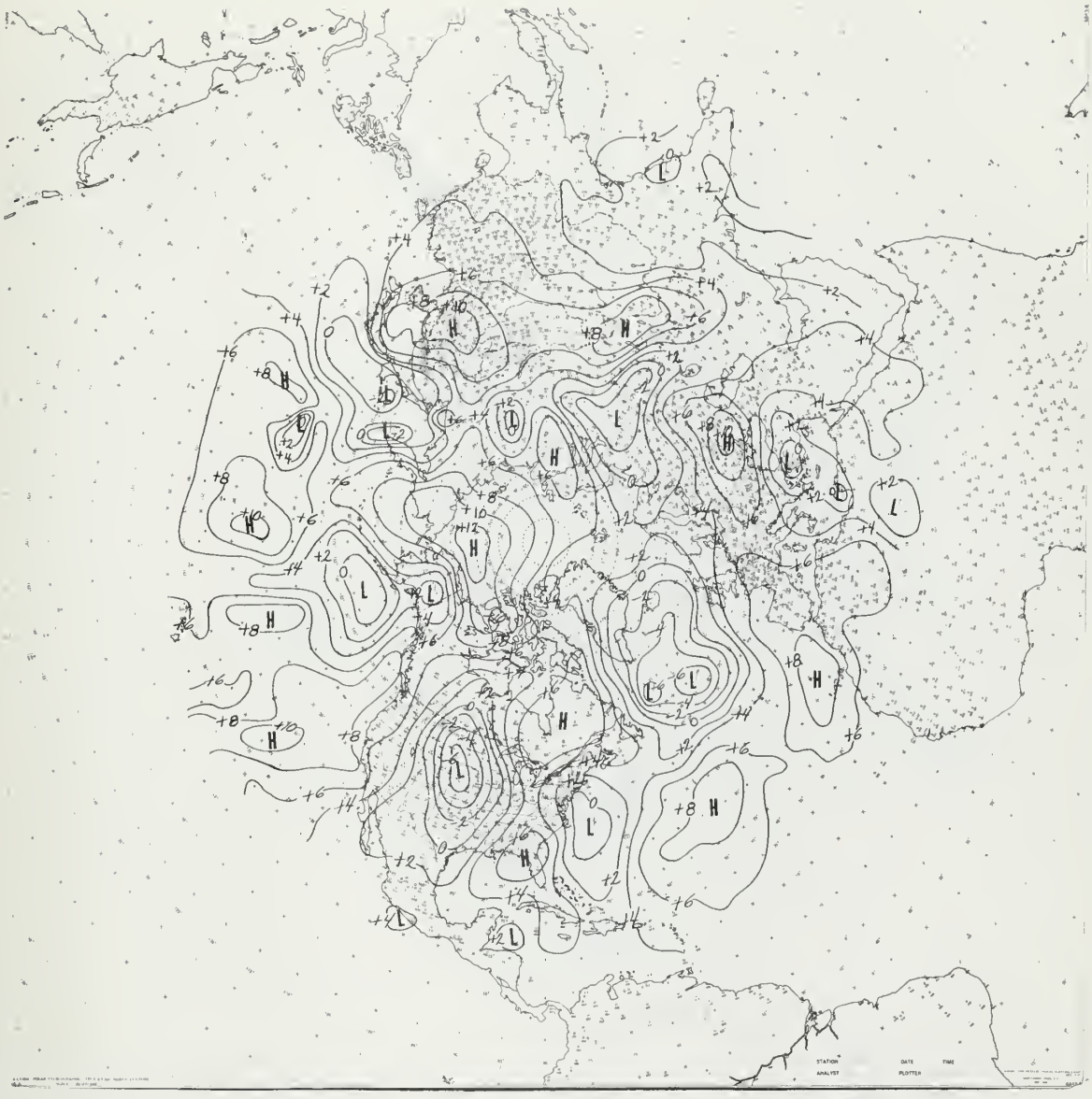

Figure 5. The 24-hr prognostic map with all three terms of the prognostic equation included.

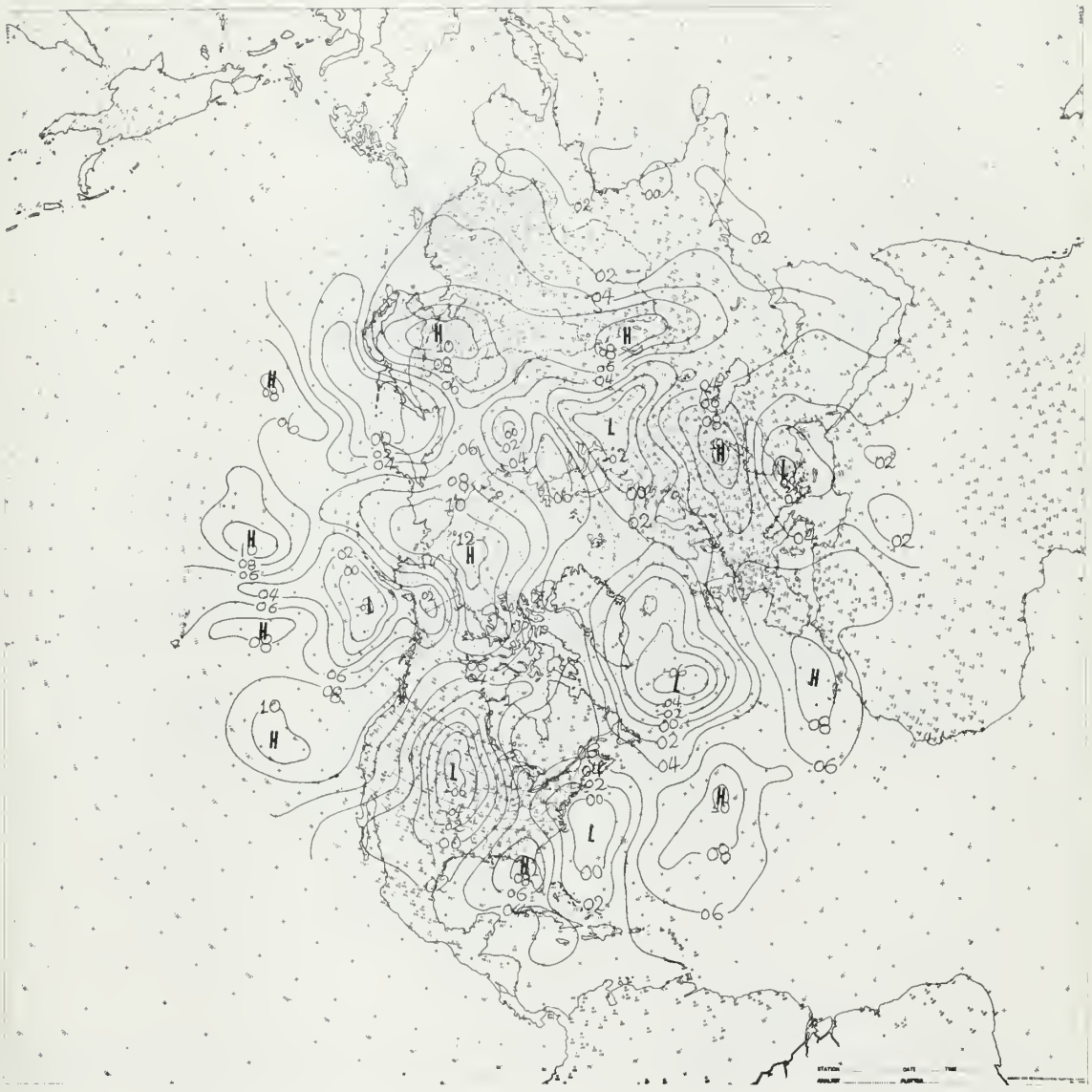

Figure 6. The 24-hr prognostic map with the thickness advection term only.

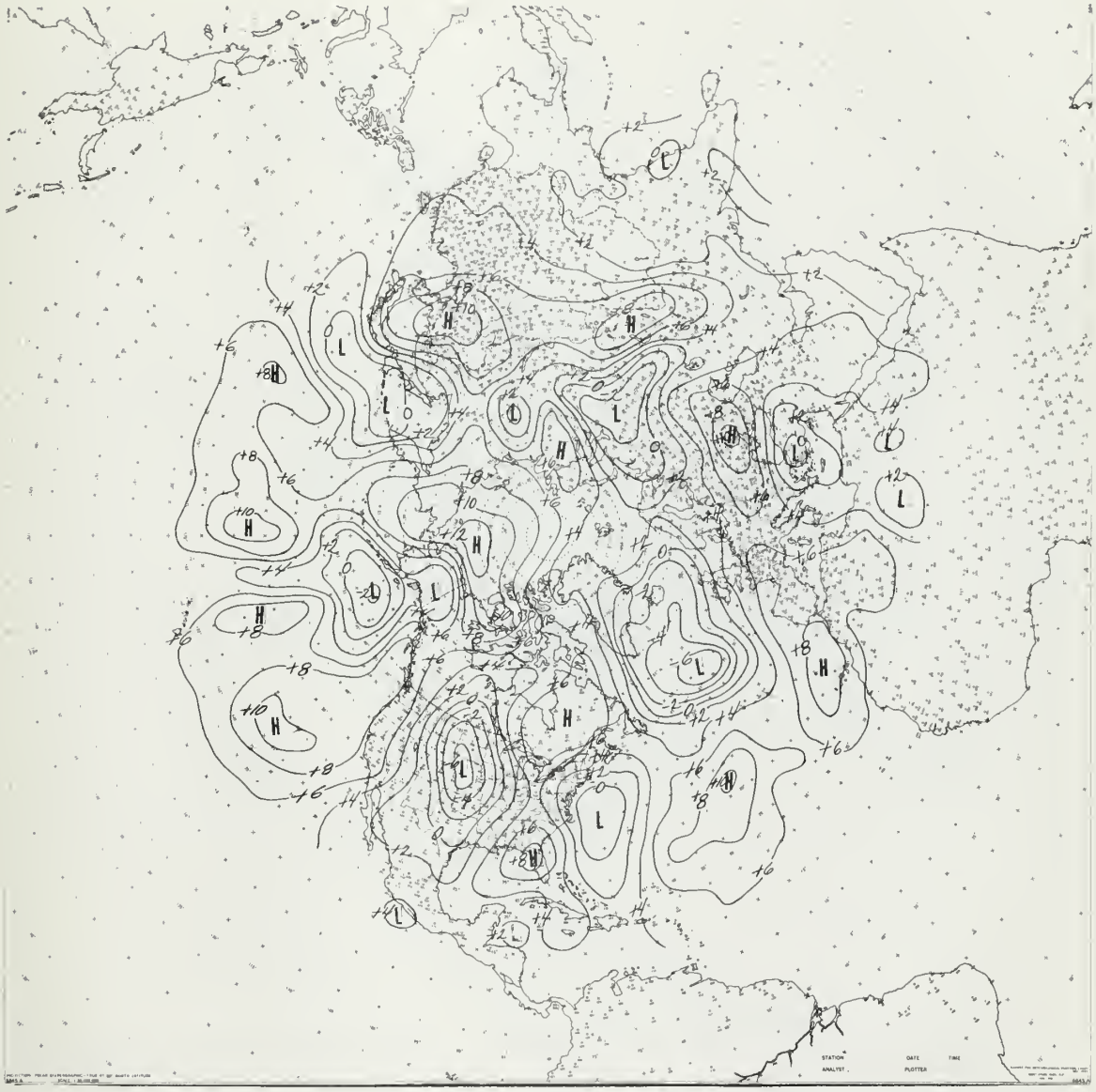

Figure 7. The 24-hr prognostic map with the thickness advection and the terrain terms.

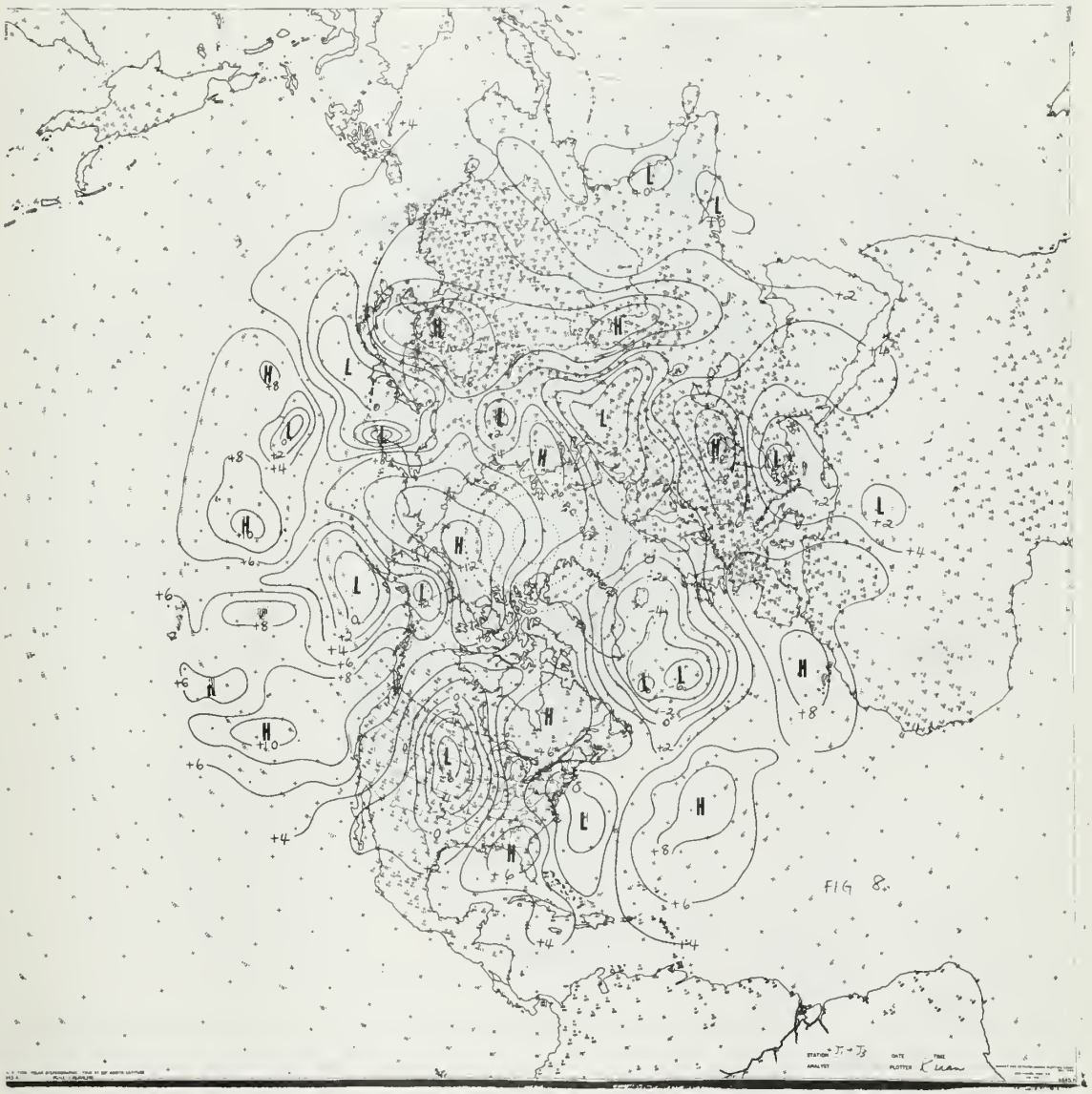

Figure 8. The 24-hr prognostic map with the thickness advection and the non-adiabatic terms.

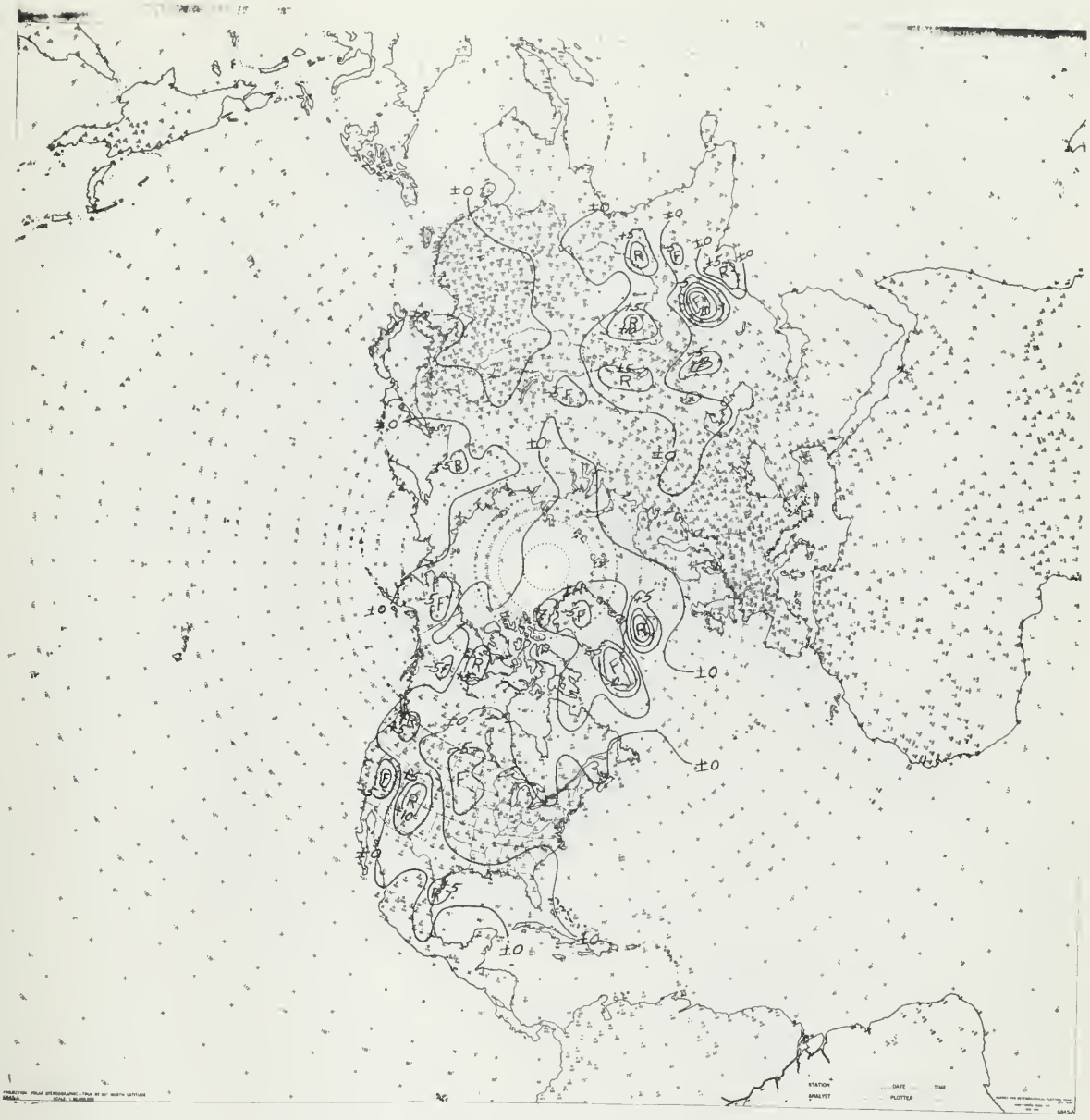

Figure 9. Analysis of the effects of the terrain term.

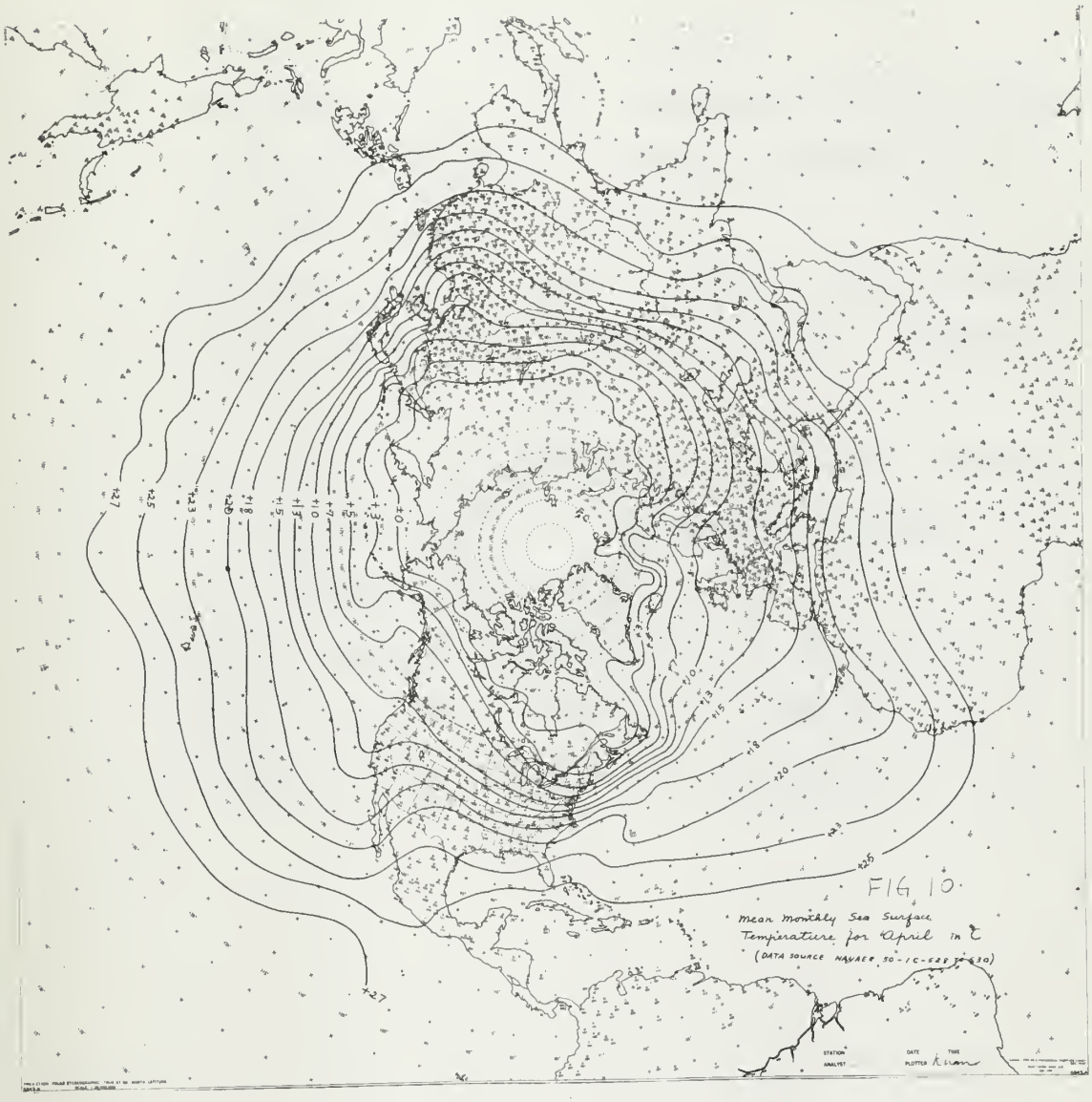

Figure 10. The monthly-mean sea-temperature field of April.

BIBLIOGRAPHY

1. Kuo, H. L., 1953: The stability properties and structure of disturbances in a baroclinic atmosphere. J. Meteor., 10, 235-243.

2. Cressman, G. P., 1960: Improved terrain effects in barotropic forecasts. Monthly Weather Review. Vol. 88, No. 9-12, 327-342.

3. Haltiner, G. J., and T. S. Hesse, 1958: Graphical prognosis including terrain effects. J. Meteor., 15, 103-107.

4. Haltiner, G. J., and Wang, Y. C., 1960: Numerical prognosis including non-adiabatic warming. J. Meteor., 17, 207-213.

5. 1956: Marine climatic atlas of the world, Vol. I, II, III. NAVAER 50-1C-528 to 530, Chief of Naval Operations, Washington, D. C.